Hindawi
Journal of Nanomaterials
Volume 2019, Article ID 9863145, 7 pages
https://doi.org/10.1155/2019/9863145

Research Article

In Situ Growth of ZnO inside a Porous Silicon Matrix Obtained by Electrochemical Etching with a Hydrofluoric Acid-Formaldehyde Solution

R. Juárez-Nahuatlato,[1] G. García,[2] M. Pacio,[2] Roberto Portillo,[3] N. Perez-Amaro,[1] F. Severiano,[4] G. Nieto,[3] T. Díaz-Becerril,[2] E. Rosendo,[2] R. Romano-Trujillo,[2] A. Coyopol,[2] and V. L. Gayou[4]

[1]*BUAP, Facultad de Ingeniería Química, Av. San Claudio s/n y 18 sur C.U. Edificio FIQ7, San Manuel C.P, 72570 Puebla, Puebla, Mexico*
[2]*BUAP, CIDS-ICUAP, Av. San Claudio s/n C.P, 72570 Puebla, Puebla, Mexico*
[3]*BUAP, Facultad de Ciencias Químicas, Av. San Claudio s/n C.P, 72570 Puebla, Puebla, Mexico*
[4]*Centro de Investigación en Biotecnología Aplicada, IPN, Ex-Hacienda San Juan Molino Carretera Estatal Tecuexcomac-Tepetitla Km 1.5, Tlaxcala C.P. 90700, Mexico*

Correspondence should be addressed to R. Juárez-Nahuatlato; rjuarez@cs.buap.mx

Received 20 June 2018; Revised 3 October 2018; Accepted 14 October 2018; Published 27 January 2019

Academic Editor: Magnus Willander

We present zinc oxide (ZnO) particles obtained inside a porous silicon matrix in the same electrolytic process using a p-type silicon wafer in a hydrofluoric acid (HF) solution containing formaldehyde (CH_2O) and hydrated zinc sulfate as additives. The X-ray diffraction pattern of the sample confirmed the presence of ZnO with a hexagonal-type wurtzite structure. Photoluminescence (PL) spectra of the samples, before and after the functionalization process, were measured to observe the effect of ZnO inside the porous silicon. The PL measurements of porous silicon functionalized with ZnO (ZnO/PS) revealed infrared, red, blue, and ultraviolet emission bands. The ultraviolet region corresponds to the band-band emission of ZnO, and the visible emission is attributed to defects. The results of the nitrogen adsorption/desorption isotherms of the PS and ZnO/PS samples revealed larger BET surface areas and pore diameters for the ZnO/PS sample. We conclude that ZnO/PS can be obtained in a one-step electrolytic process. These types of samples can be used in gas sensors and photocatalysis.

1. Introduction

In recent years, zinc oxide (ZnO) has been investigated as a functional material for electronic and optoelectronic devices such as gas sensors [1, 2], photodetectors [3], solar cells [4], and laser diodes [5]. Nanostructures of ZnO have been observed with a variety of forms: nanorods, nanowires, nanobelts, and nanosheets [6, 7]. The advantages of nanostructures include their high surface/volume ratio and good chemical and thermal stability. These nanostructures typically exhibit photoluminescence (PL) spectra of ZnO composed of a visible blue, green, and red bands related to a level defect emission and ultraviolet band-band emission [8]. At room temperature, ZnO is an important semiconductor with a wide band gap of 3.36 eV. Additionally, the discovery of PL at room temperature (RT) in the visible spectral region from porous silicon (PS) has resulted in a great deal of research [9]. In recent years, much effort has been focused on nanocomposites based on PS due to its potential applications in silicon-based optoelectronic devices. The high surface/volume ratio of PS renders it favorable as a possible matrix for a variety of nanoparticles for various applications [10]. We believe that the functionalization of PS with ZnO paves the way for integrating ZnO into integrated circuits based

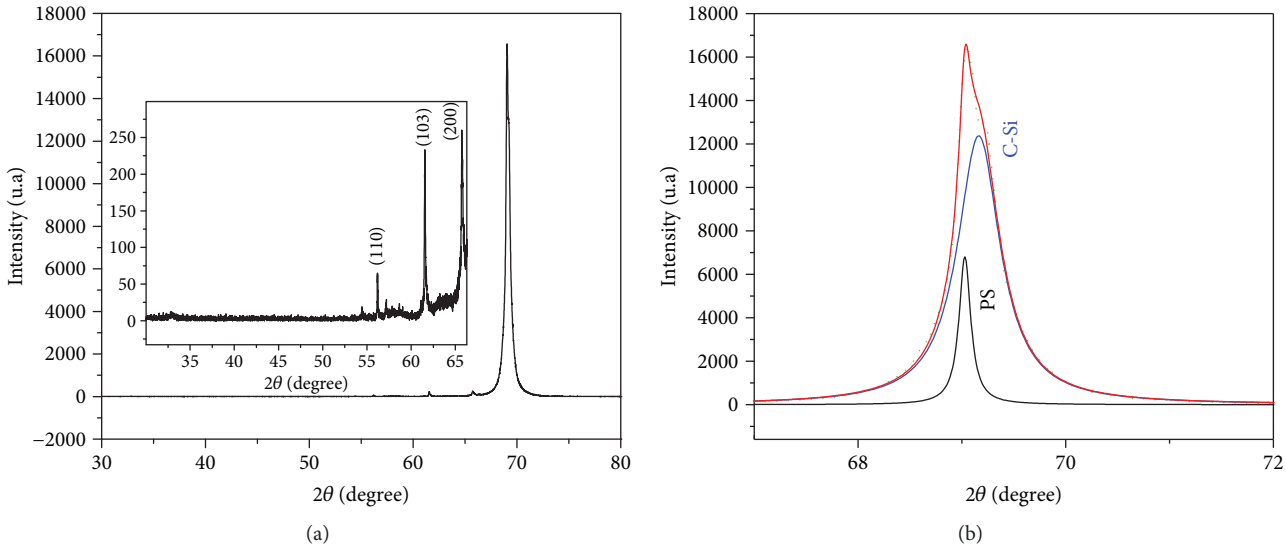

FIGURE 1: (a) XRD patterns of ZnO/PS. The inset shows the expanded view of the (110), (103), and (200) diffraction peaks corresponding to the ZnO planes. (b) Multi-Gaussian fitting of the XRD patterns between 67° and 72°. The green dotted line corresponds to the experimental data, and the red line is the sum of the two contributions, which consist of the crystalline silicon substrate peak (C-Si) and the PS layer.

on silicon [11]. To deposit ZnO particles on PS, different methods have been proposed such as radio frequency (RF) magnetron sputtering [12], sol-gel [13], plasma-assisted molecular beam epitaxy (PA-MBE) [14], and electrochemical deposition [15].

ZnO films on silicon substrates result in a large stress between the ZnO and silicon due to the significant mismatch in the thermal expansion coefficients and lattice constants of these materials [16]. On the other hand, the sponge-like open structure and large specific surface area make PS a convenient material for depositing ZnO and therefore establishing a nucleation site that is essential for ZnO deposition.

In this study, PS and ZnO/PS were obtained via electrochemical anodization. The PS was characterized by PL, nitrogen adsorption/desorption isotherm, and gravimetry. The ZnO/PS was characterized by X-ray measurements (XRD), PL, nitrogen adsorption/desorption isotherm, and gravimetry. The ZnO/PS was made without a catalyzer.

2. Materials and Methods

The PS was obtained using wafers of p-type crystalline silicon with an orientation of <100> and an electrical resistivity of 0.01–0.02 Ω·cm in a teflon reactor in which the cathode was a tungsten wire. We used a mixture of hydrofluoric acid (HF) (J.T.Baker 48%; J.T.Baker Chemical Company, Mexico) and CH_2O formaldehyde (37%, Merck KGaA; Merck Company, Mexico) in a ratio 1 : 1 as an electrolyte. We used a current density of 33.50 mA/cm^2, and the anodization process took 16.66 minutes. The porosity and thickness of PS were 50% and 50 μm, respectively. The porosity and thickness were calculated using the equations of the gravimetric method characterization [17, 18]. To obtain ZnO/PS, we first prepared the ZnO using hydrated zinc sulfate ($Zn(SO_4)\cdot 7H_2O$) in a solution (1 mM) (MEYER 97%; Química Suastes, Mexico) and sodium hydroxide (NaOH) (MEYER 97%) in an solution (1 mM). Next, we mixed the solutions for 4 hours and stored them at 100°C; this solution was labeled "ZnO." This solution was then mixed with HF and CH_2O to obtain $HF : CH_2O : ZnO$ in a proportion of 1 : 1 : 1/2. The current density and duration of the process were 29.81 mA/cm^2 and 26.40 minutes, respectively. The porosity was 50% and the thickness was 50 μm. The XRD pattern of ZnO/PS was obtained using a Bruker D8 ADVANCE diffractometer (Bruker Corporation, http://www.bruker.com) with Cu Kα ($\lambda = 1.546$ Å). The pattern was obtained over an interval of 30–80° in steps of 0.02°. The PL measurements were obtained using a Cary Eclipse (Fluorescence-Spectrophotometer; Agilent Technologies, http://www.agilent.com) with an Xe lamp as the excitation source ($\lambda = 325$ nm). The porous characteristics were determined using a Quantachrome AS-1C equipment that enabled measurements of the isotherm adsorption-desorption of nitrogen over the adsorbent materials. Macroscopic characteristics such as porosity and thickness were calculated using the gravimetric method. The gravimetric technique was carried out using mass measurements: the wafer was weighed before anodization, just after anodization and after a rapid dissolution of the whole porous layer in a 2% NaOH solution. Each sample was tested at least two times, and the average value was recorded. Furthermore, a current density between 20 and 60 mA/cm^2 was applied over an exposed area of 1.762 cm^2 over 60 minutes. We used a Keithley power source model 2400C (Keithley Instruments Inc., http://www.keithley.com) in constant-current mode.

3. Results and Discussion

3.1. Structural Characterization. We used XRD to investigate the crystal phase of the samples. Figure 1(a) shows that the ZnO was electrodeposited over the PS. The ZnO obtained was polycrystalline, the diffraction planes were (110), (103),

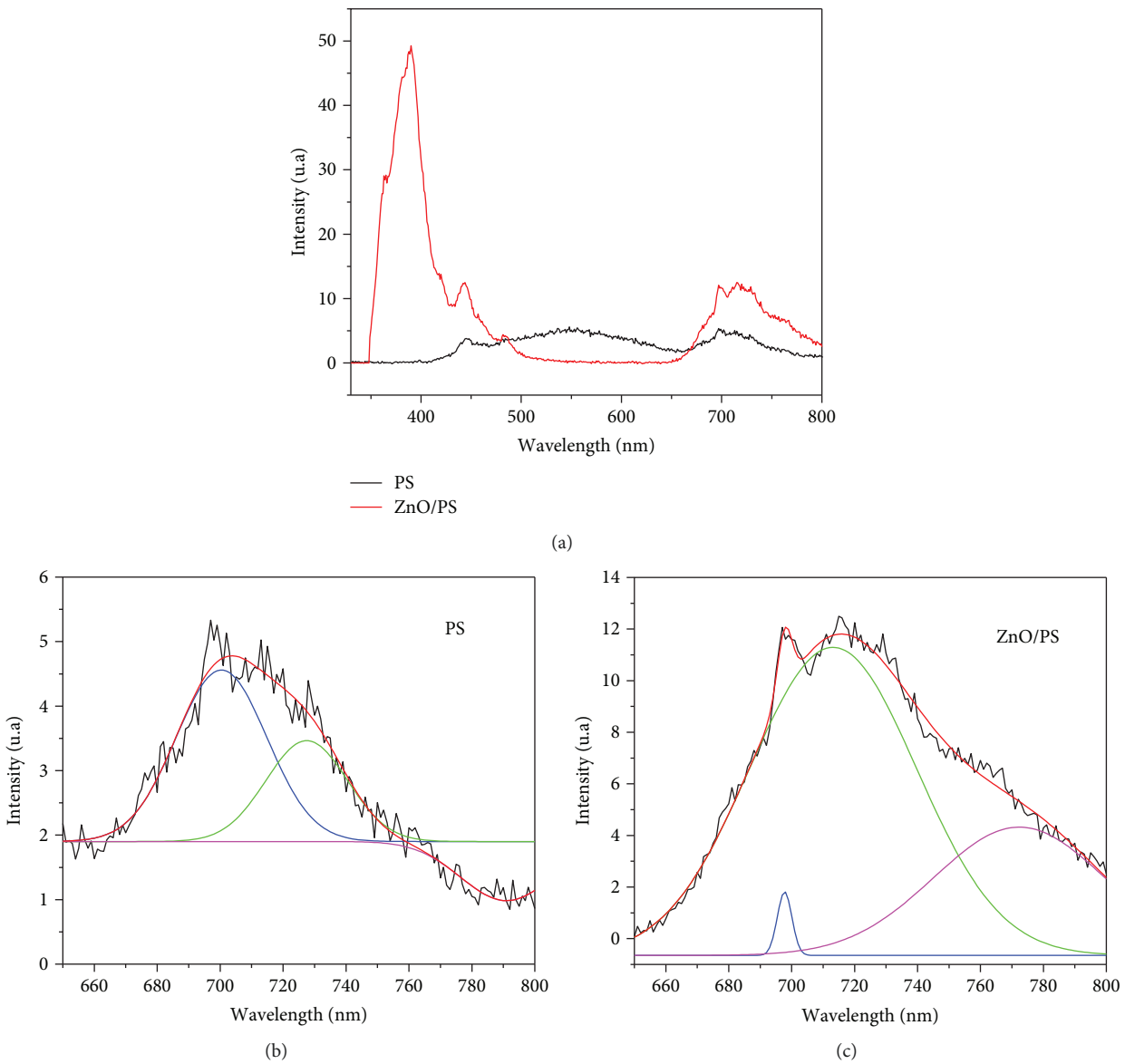

Figure 2: (a) Room temperature PL of PS and ZnO/PS. (b) Multi-Gaussian fitting of PL spectra from the PS sample: the red line is the sum of the three contributions (blue, green, and pink lines), and the black line corresponds to the experimental data. (c) Multi-Gaussian fitting of PL spectra from the ZnO/PS sample: the red line is the sum of the tree contributions (blue, green, and pink lines), and the black line corresponds to the experimental data.

and (200), and the sample exhibited a wurtzite-type hexagonal crystalline structure with spatial group P63mc (JCPDS No. 36-1451). The inset figure in Figure 1(a) shows the enlargement of the diffraction peaks of ZnO. The pattern region between 67° and 72° was fit with two Gaussian components (Figure 1(b)) related to the crystal phase of substrate (observed at $2\theta = 69.17°$ (JCPDS 00-027-1402)) and the PS at $2\theta = 69.02°$, respectively.

3.2. Optical Properties

3.2.1. Photoluminescence. The black line in Figure 2(a) indicates the PL spectrum of the PS layer exhibiting PL emission bands at 444, 548, and 684 nm. The band of luminescence centered at 444 nm has been reported in electrochemically etched PS followed by an oxidation process; the emission from silicon oxide model, widely accepted, suggests that different types of defects in silicon oxide may be responsible for PL. This idea has gained support based on the correlation between the intensity of the blue PL band and the intensity of peak, obtained by Fourier-transform infrared spectroscopy (FTIR), corresponding to the Si-O bond [19, 20]. We suggest that the blue PL is due to SiO_X defects. The band of luminescence centered at 548 nm may be associated with the complex nature of the surface states present on the large internal surface of the PS [21]. The PL emission band from 620–800 nm originates from the quantum confinement of electrons in the nanocrystals of silicon in PS [22].

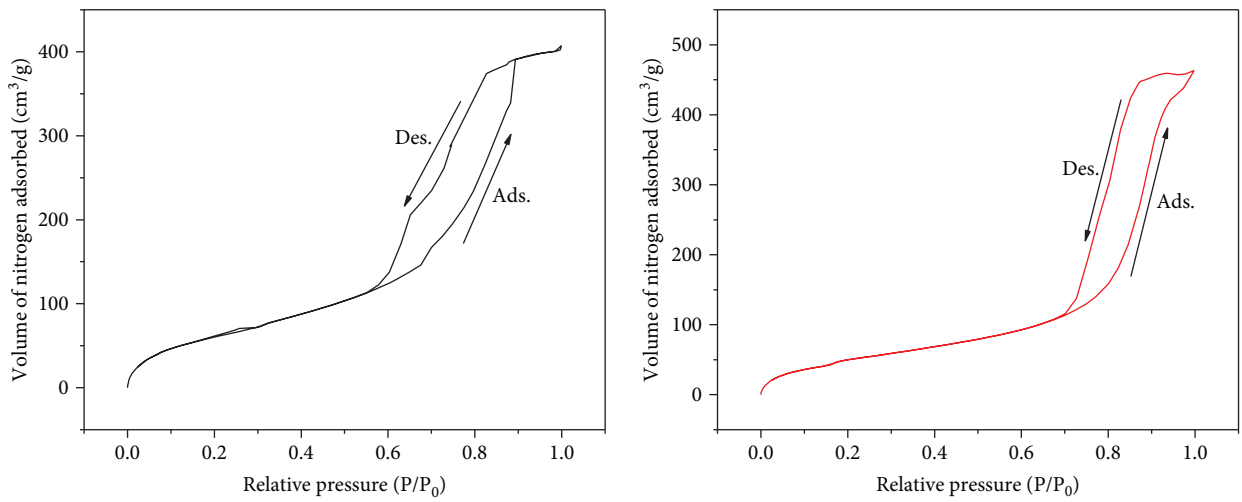

Figure 3: Nitrogen adsorption/desorption (ads./des.) isotherms at 77 K, (a) PS and (b) ZnO/PS.

In order to explain our results, in this oxygen-rich condition, the amount of oxygen that diffuses into the sample increases. Therefore, the types of defects most frequently found in ZnO grown under O-rich conditions are intrinsic defects such as interstitial oxygen (O_i), zinc vacancies (V_{Zn}), and antisite oxygen (O_{Zn}).

The red line in Figure 2(a) indicates the PL spectrum of the ZnO/PS layer that exhibits ultraviolet blue, red, and infrared regions. The emission around 388 nm corresponds to the band-band emission of ZnO [23]. Furthermore, there is the emission band at 445–490 nm that has been observed in ZnO regardless of morphology. The mechanism suggested to explain this luminescence is associated with zinc vacancies V_{Zn}, which are usually attributed to transitions from the conduction band to zinc vacancies V_{Zn} [24]. We observed the following characteristics from 650–800 nm (Figure 2(a)): a broad band and an asymmetric shape. According to these characteristics, the spectral region was fit with three Gaussian components to determine the predominant mechanism responsible for the optical emission. We expect that the measured spectrum is the result of the superposition of one or more luminescence bands. We can accordingly explain, in a qualitative way, the PL spectra and their dependence on the growth conditions of the sample. Finally, our use of Gaussian fitting allowed us to compare our results with those in the literature. The results of this fitting procedure are shown in Figure 2(b) for PS. We noted the presence of two well-determined luminescence bands: a band of luminescence centered at 700 nm and another band of luminescence centered at 727 nm. As discussed above, the origin of these bands is due to quantum confinement in PS [22]. Similarly, for the ZnO/PS shown in Figure 2(c), the presence of three well-determined luminescence bands was observed: two at 698 nm and 712 nm corresponding to the quantum confinement of electrons in the nanocrystals of silicon in PS [22] and another centered at 774 nm that has been related to oxygen defects such as O_i and O_{Zn} [25–27]. These defects O_i and O_{Zn} are formed during the growth process due to the oxygen-rich conditions [26].

When the PS is functionalized with ZnO, the PL intensity in the ultraviolet and red-infrared regions increases (Figure 2(a)). The increase in the ultraviolet region is due to the ZnO deposited into the PS. In the red-infrared region, the increase can indicate that PS nanocrystallites are changing in structure given the ZnO deposition [22]. Therefore, we believe that the deposition of ZnO onto PS stabilizes the nonradiative states or free bonds. Radiative recombination of photoexcited carriers should occur via relaxed electronic states, possibly oxygen-related defect states at the interface between PS and ZnO. Therefore, we suggest that the nonradiative states on the PS surface can be replaced during oxidation due to the electrodeposition of ZnO. This process results in an increase in PL intensity in the ultraviolet and red-infrared regions. On the other hand, oxygen vacancies are unlikely to form during the electrodeposition of ZnO under the conditions noted above. In addition to disappearing complex states, the luminescence (green-orange) caused by this defect consequently decreases.

3.3. Isotherms. The PS and ZnO/PS samples were texturally characterized by nitrogen physisorption. Figures 3(a) and 3(b) show the adsorption/desorption isotherms measured at the boiling temperature of liquid nitrogen (77 K), which represent the volume of nitrogen adsorbed under STP conditions as a function of relative pressure. According the IUPAC classification, the adsorption isotherms are type IV and characteristic of mesoporous solids [28].

In addition, the adsorption/desorption isotherms exhibit a type H1 hysteresis cycle that is associated with materials with pores with homogeneous shapes and sizes and narrow pore size distributions. The pore size distribution was evaluated using the Barret-Joyner-Halenda (BJH) and density functional (DFT) methods. This work confirmed the presence of mesoporosity in the PS and ZnO/PS materials. Considering that multilayer adsorption results in capillary condensation on a cylindrical mesopore at a given relative pressure, the pore size can be determined applying the Kelvin equation [28]:

$$\ln \frac{P}{P_0} = \frac{2\sigma v_m \cos\theta}{r_\kappa RT}, \quad (1)$$

where P/P_0 is the relative pressure of nitrogen, r_κ is the Kelvin radius, σ is the surface tension, and v_m is the molar volume of liquid nitrogen (34.7 cm^3/mol). R (8.314×10^7 erg/mol*K and T = 77 K have their usual definitions.

Using the constants for nitrogen, equation (1) reduces to

$$r_\kappa = \frac{4.15}{\log P_o/P}. \quad (2)$$

The Kelvin radius is the radius of the meniscus of the adsorbable condensed within the cylindrical pore at a relative pressure P/P_0. It is assumed that adsorption occurs via a monolayer-multilayer mechanism until capillary condensation occurs in medium-sized pores. Prior to condensation, some multilayer adsorption has taken place on the wall of the pore. As a result, r_κ does not represent the actual pore radius. Conversely, during desorption an adsorbed multilayer remains on the walls when evaporation of the liquid adsorbate occurs. The actual pore radius r_p is given by $r_p = r_\kappa + t$, where t is the thickness of the adsorbed multilayer.

From the adsorption data determined experimentally, we also calculated the surface specific of the material using the Brunauer-Emmett-Teller (BET) model [29]:

$$\frac{P}{V(1-(P/P_0))} = \frac{1}{V_{mon}C} + \frac{C-1}{V_{mon}C}\frac{P}{P_0}, \quad (3)$$

where V_{mon} is the volume of gas adsorbed per unit mass in a monolayer, V is the volume of gas adsorbed per unit mass of the sample, C is a parameter related to the enthalpy molar of adsorption, and P_0 is the saturated vapor pressure of liquid nitrogen at 77 K. Equation (3) has been used in gas adsorption/desorption isotherms in porous matrices to determine the V_{mon} and the constant BET (C) from the slope and the intercept of the straight line obtained from a plot of $P/V(1-(P/P_0))$ as a function of P/P_0. The monolayer capacity (V_{mon}) is used to calculate the specific surface area of a material. The values of these textural properties, reported in Table 1, suggest the possible application of these materials in gas sensor devices and in photocatalysis [30].

3.4. Gravimetry. We used the gravimetric method to obtain the porosity and etching rate of the PS samples with and without ZnO [17]. In Figure 4, we can note a similar porosity behavior for both electrolyte solutions ($HF:CH_2O:ZnO$ and $HF:CH_2O$). Figure 5 shows that the etching rate decreases for the same electrical current conditions with the $HF:CH_2O:ZnO$ solution; the etching rate decreases can be attributed to the metal effect of Zn because it acts as a catalyst. It has been reported that the presence of a metal changes the etching rate from that of a silicon substrate in an M/HF (M = metal) solution [31]. Metal-assisted chemical etching was closely investigated by Li and Bond. These authors found that given a tiny layer of metal particles (e.g., Au and Pt) exposed over a silicon layer, the silicon attack was catalyzed in a solution of $HF\text{-}CH_3CH_2OH$, yielding long pores [31].

Hole injection is well documented for the oxidation and dissolution of silicon in metal-assisted chemical etching of Si [31–34]. In this process, the metal acts as a microscopic cathode when the oxidation of silicon occurs. The metallic

Table 1: Data obtained from the adsorption/desorption isotherms.

Sample	Pore diameter (nm)	Porosity (%)	Surface area (m^2/g)
PS	5.86	50	237.90
ZnO/PS	8.19	50	294.00

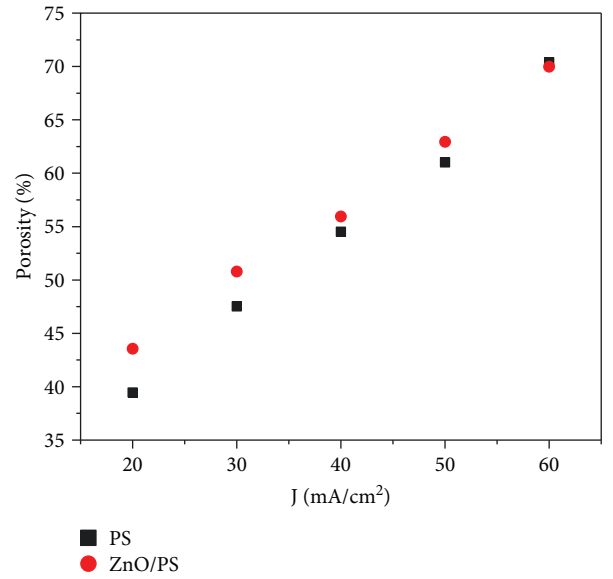

Figure 4: Porosity as a function of the applied current density for PS and ZnO/PS.

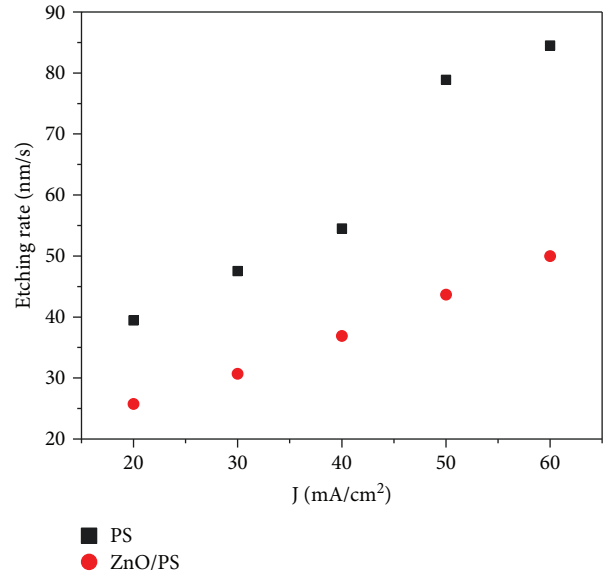

Figure 5: Etching rate as a function of the applied current density for PS and ZnO/PS.

ions (Zn^{+2}) are reduced, which yields electrons from the Si-Si bond over the layer of silicon. In a Zn/HF solution, the charge transfer necessary for the oxidation and dissolution of Si is carried out, which is similar to the M/HF solution. In this way, the etching rate changes between silicon and a solution containing $HF:CH_2O$; this effect can be seen in Figure 5.

A similar behavior can be observed for both electrolytes if increasing the current density increases the porosity (Figure 4). This figure shows that for a certain fixed current density, the porosity of PS and ZnO/PS is nearly identical. Figure 5 shows that for a fixed current density, the etching rate decreases when the $HF:CH_2O:ZnO$ solution is used; this finding may be due to the effect of the Zn.

4. Conclusions

ZnO was deposited and pores were formed simultaneously during the electrochemical anodization. The presence of ZnO inside the PS matrix was confirmed by XRD. Ultraviolet and red emissions of ZnO inside the PS were verified by PL. We suggest that the optical properties of ZnO/PS were enhanced by the functionalization process. Pore formation was demonstrated for nitrogen adsorption/desorption isotherms, proving the formation of a mesoporous material. Obtaining PS functionalized with ZnO was carried out at RT in step one of the electrolytic process.

Data Availability

The data used to support the findings of this study are available from the corresponding author upon request.

Conflicts of Interest

The authors declare that they have no conflicts of interest.

Acknowledgments

R. Juárez-Nahuatlato acknowledges CONACyT for a fellowship (CVU: 88178); funding was provided by VIEP-BUAP projects.

References

[1] M. Z. Ahmad, J. Chang, M. S. Ahmad, E. R. Waclawik, and W. Wlodarski, "Non-aqueous synthesis of hexagonal ZnO nanopyramids: gas sensing properties," *Sensors and Actuators B: Chemical*, vol. 177, pp. 286–294, 2013.

[2] O. Lupan, V. Postica, J. Gröttrup et al., "Hybridization of zinc oxide tetrapods for selective gas sensing applications," *ACS Applied Materials & Interfaces*, vol. 9, no. 4, pp. 4084–4099, 2017.

[3] H. Zhou, G. Fang, N. Liu, and X. Zhao, "Ultraviolet photodetectors based on ZnO nanorods-seed layer effect and metal oxide modifying layer effect," *Nanoscale Research Letters*, vol. 6, no. 1, p. 147, 2011.

[4] R. Pietruszka, B. S. Witkowski, E. Zielony, K. Gwozdz, E. Placzek-Popko, and M. Godlewski, "ZnO/Si heterojunction solar cell fabricated by atomic layer deposition and hydrothermal methods," *Solar Energy*, vol. 155, pp. 1282–1288, 2017.

[5] C. Chen, J. Zhang, J. Chen et al., "Near-ultraviolet electroluminescence from ZnO-based light-emitting diodes with n-ZnO nanorod/p-GaN direct-bonding heterojunction structure," *Materials Letters*, vol. 189, pp. 144–147, 2017.

[6] S. Öztürk, N. Kılınç, N. Taşaltin, and Z. Z. Öztürk, "A comparative study on the NO_2 gas sensing properties of ZnO thin films, nanowires and nanorods," *Thin Solid Films*, vol. 520, no. 3, pp. 932–938, 2011.

[7] J. Li, H. Fan, and X. Jia, "Multilayered ZnO nanosheets with 3D porous architectures: synthesis and gas sensing application," *Journal of Physical Chemistry C*, vol. 114, no. 35, pp. 14684–14691, 2010.

[8] V. A. Fonoberov, K. A. Alim, A. A. Balandin, F. Xiu, and J. Liu, "Photoluminescence investigation of the carrier recombination processes in ZnO quantum dots and nanocrystals," *Physical Review B*, vol. 73, no. 16, article 165317, 2006.

[9] M. V. Wolkin, J. Jorne, P. M. Fauchet, G. Allan, and C. Delerue, "Electronic states and luminescence in porous silicon quantum dots: the role of oxygen," *Physical Review Letters*, vol. 82, no. 1, pp. 197–200, 1999.

[10] L. Luo, X. X. Zhang, K. F. Li et al., "Er/Yb doped porous silicon—a novel white light source," *Advanced Materials*, vol. 16, no. 18, pp. 1664–1667, 2004.

[11] G. T. A. Kovacs, N. I. Maluf, and K. E. Petersen, "Bulk micromachining of silicon," *Proceedings of the IEEE*, vol. 86, no. 8, pp. 1536–1551, 1998.

[12] H. Cai, H. Shen, Y. Yin, L. Lu, J. Shen, and Z. Tang, "The effects of porous silicon on the crystalline properties of ZnO thin films," *Journal of Physics and Chemistry of Solids*, vol. 70, no. 6, pp. 967–971, 2009.

[13] N. Kitazawa, M. Aono, and Y. Watanabe, "Growth of vertically aligned one-dimensional ZnO nanowire arrays on sol-gel derived ZnO thin films," *Journal of Physics and Chemistry of Solids*, vol. 75, no. 11, pp. 1194–1200, 2014.

[14] M. S. Kim, K. G. Yim, J. Y. Leem et al., "Thickness dependence of properties of ZnO thin films on porous silicon grown by plasma-assisted molecular beam epitaxy," *Journal of the Korean Physical Society*, vol. 59, no. 3, pp. 2354–2361, 2011.

[15] D. Yan, S. Li, S. Liu, M. Tan, D. Li, and Y. Zhu, "Electrochemical synthesis of ZnO nanorods/porous silicon composites and their gas-sensing properties at room temperature," *Journal of Solid State Electrochemistry*, vol. 20, no. 2, pp. 459–468, 2016.

[16] H.-C. Hsu, C. S. Cheng, C. C. Chang, S. Yang, C. S. Chang, and W. F. Hsieh, "Orientation-enhanced growth and optical properties of ZnO nanowires grown on porous silicon substrates," *Nanotechnology*, vol. 16, no. 2, pp. 297–301, 2005.

[17] N. S. Subramanian, R. V. Sabaapathy, P. Vickraman, G. V. Kumar, R. Sriram, and B. Santhi, "Investigations on Pd:SnO_2/-porous silicon structures for sensing LPG and NO_2 gas," *Ionics*, vol. 13, no. 5, pp. 323–328, 2007.

[18] O. Bisi, S. Ossicini, and L. Pavesi, "Porous silicon: a quantum sponge structure for silicon based optoelectronics," *Surface Science Reports*, vol. 38, no. 1-3, pp. 1–126, 2000.

[19] A. J. Kontkiewicz, A. M. Kontkiewicz, J. Siejka et al., "Evidence that blue luminescence of oxidized porous silicon originates from SiO_2," *Applied Physics Letters*, vol. 65, no. 11, pp. 1436–1438, 1994.

[20] Q. W. Chen, D. L. Zhu, C. Zhu, J. Wang, and Y. G. Zhang, "A way to obtain visible blue light emission in porous silicon," *Applied Physics Letters*, vol. 82, no. 7, pp. 1018–1020, 2003.

[21] C. Lee, K. Kim, and K. Prabakar, "Characterization of ZnO:Al-thin-film-passivated porous silicon," *Journal of the Korean Physical Society*, vol. 48, no. 6, pp. 1193–1198, 2006.

[22] K. Herynková, M. Šlechta, P. Šimáková, A. Fučíková, and O. Cibulka, "Agglomeration of luminescent porous silicon nanoparticles in colloidal solutions," *Nanoscale Research Letters*, vol. 11, no. 1, pp. 367–365, 2016.

[23] Y. Zhang, J. Xu, Q. Xiang, H. Li, Q. Pan, and P. Xu, "Brush-like hierarchical ZnO nanostructures: synthesis, photoluminescence and gas sensor properties," *Journal of Physical Chemistry C*, vol. 113, no. 9, pp. 3430–3435, 2009.

[24] C. H. Ahn, Y. Y. Kim, D. C. Kim, S. K. Mohanta, and H. K. Cho, "A comparative analysis of deep level emission in ZnO layers deposited by various methods," *Journal of Applied Physics*, vol. 105, no. 1, article 013502, 2009.

[25] R. K. Biroju and P. K. Giri, "Strong visible and near infrared photoluminescence from ZnO nanorods/nanowires grown on single layer graphene studied using sub-band gap excitation," *Journal of Applied Physics*, vol. 122, no. 4, article 044302, 2017.

[26] M. Wang, Y. Zhou, Y. Zhang, E. Jung Kim, S. Hong Hahn, and S. Gie Seong, "Near-infrared photoluminescence from ZnO," *Applied Physics Letters*, vol. 100, no. 10, article 101906, 2012.

[27] A. Janotti and C. G. Van de Walle, "Native point defects in ZnO," *Physical Review B*, vol. 76, no. 16, article 165202, 2007.

[28] K. S. W. Sing, D. H. Everett, R. A. W. Haul et al., "Reporting Physisorption data for gas/solid systems with special reference to the determination of surface area and porosity," *Pure and Applied Chemistry*, vol. 57, no. 4, pp. 603–619, 1985.

[29] S. Brunauer, P. H. Emmett, and E. Teller, "Adsorption of gases in multimolecular layers," *Journal of the American Chemical Society*, vol. 60, no. 2, pp. 309–319, 1938.

[30] Y. Qu, X. Zhong, Y. Li, L. Liao, Y. Huang, and X. Duan, "Photocatalytic properties of porous silicon nanowires," *Journal of Materials Chemistry*, vol. 20, no. 18, pp. 3590–3594, 2010.

[31] X. Li and P. W. Bohn, "Metal-assisted chemical etching in HF/H_2O_2 produces porous silicon," *Applied Physics Letters*, vol. 77, no. 16, pp. 2572–2574, 2000.

[32] K. Q. Peng, Y. J. Yan, S. P. Gao, and J. Zhu, "Dendrite assisted growth of silicon nanowires in electroless metal deposition," *Advanced Functional Materials*, vol. 13, no. 2, pp. 127–132, 2003.

[33] T. Hadjersi, N. Gabouze, E. S. Kooij et al., "Metal-assisted chemical etching in $HF/Na_2S_2O_8$ or $HF/KMnO_4$ produces porous silicon," *Thin Solid Films*, vol. 459, no. 1-2, pp. 271–275, 2004.

[34] K. Tsujino and M. Matsumura, "Boring deep cylindrical nanoholes in silicon using silver nanoparticles as a catalyst," *Advanced Materials*, vol. 17, no. 8, pp. 1045–1047, 2005.